PCCP

Accepted Manuscript

ROYAL SOCIETY OF CHEMISTRY

www.rsc.org/pccp

Proton transfer in short hydrogen bonded complex caused by solvation shell fluctuations: ab initio MD and NMR/UV study of an $(OHO)^-$ bonded system

Svetlana Pylaeva,[1] Christoph Allolio,[2] Benjamin Koeppe,[3] Gleb S. Denisov,[1] Hans-Heinrich Limbach,[3] Daniel Sebastiani,[4] Peter M. Tolstoy[1,5*]

[1] Department of Physics, St. Petersburg State University, Ulianovskaya st. 3, 198504 St.Petersburg, Russia

[2] Institute of Organic Chemistry and Biochemistry, Academy of Sciences of the Czech Republic, Flemingovo nám. 2, 16610 Prague 6, Czech Republic

[3] Institute of Chemistry and Biochemistry, Freie Universität Berlin, Takustrasse 3, 14195 Berlin, Germany

[4] Institute of Chemistry, Martin-Luther Universität Halle-Wittenberg, Von-Danckelmann-Platz 4, 06120 Halle, Germany

[5] Department of Chemistry, St. Petersburg State University, Universitetsky pr. 26, 198504 St.Petersburg, Russia

Abstract

We present a joint experimental and quantum chemical study on the influence of solvent dynamics on the protonation equilibrium in a strongly hydrogen bonded phenol-acetate complex in CD_2Cl_2. Particular attention is given to the correlation of the proton position distribution with the internal conformation of the complex itself and with fluctuations of the aprotic solvent. Specifically, we have focused on a complex formed by 4-nitrophenol-tetraalkylammonium-acetate in CD_2Cl_2. Experimentally we have used

combined low-temperature ^{1}H and ^{13}C NMR and UV-vis spectroscopy and showed that very strong OHO hydrogen bond is formed with proton tautomerism (PhOH···$^{-}$OAc and PhO^{-}···HOAc forms, both strongly hydrogen bonded). Computationally, we have employed *ab initio* molecular dynamics (70 and 71 solvent molecules, with and without the presence of counter-cation, respectively). We demonstrate that the relative motion of counter-cation and "free" carbonyl group of the acid plays the major role in the OHO bond geometry and causes proton "jumps", *i.e.* interconversion of PhOH···$^{-}$OAc and PhO^{-}···HOAc tautomers. Weak H-bonds between CH(CD) groups of the solvent and oxygen atom of carbonyl stabilize PhOH···$^{-}$OAc type of structures. Breaking of CH···O bonds shifts the equilibrium towards PhO^{-}···HOAc form.

1. Introduction

Geometries of hydrogen-bonded complexes in solutions are often an elusive subject, to a big extent owing to their fluxional nature. For a given pair of partners a small change in the local environment might induce a large change in the structure of the complex.[1, 2] In the solid state the interaction with the medium is provided by crystal packing,[3] while in a hydrophobic pocket of a protein it is due to the polar groups in the proximity of the hydrogen bridge.[4] In solution the main interactions come from the first solvation shell.[5-8] Thermal fluctuations within the complex and its medium lead to a constant re-arrangement of the H-bond geometry and a distribution of rapidly interconverting structures is likely to be created.[7, 9] For systems in liquid state this is sometimes called "solvatomerism".[10, 11] The lifetime of a solvatomer is limited by the rotational diffusion time and usually does not exceed 10^{-9} s (often it lies in picosecond time scale).[12-19]

Depending on the interacting partners and conditions several situations could be realized. In some cases the distribution of the geometries in an AHB complex would be sufficiently narrow and well represented by a single structure (Fig. 1a).[20] In some other cases the distribution would contain two clearly distinct groups of structures, referred to as proton tautomers, A-H···B $\rightleftharpoons$ A···H-B (Fig. 1b).[7, 10, 11, 21] Perhaps the most classical type of intermolecular complex with proton tautomerism is carboxylic acid – pyridine system.[22-26] In intermediate cases, often occurring in short strong H-bonds, for the correct description the

whole proton distribution function should be considered (Fig. 1c).[27,28] Or course, there is also quantum delocalization due to the zero-point vibrations. Throughout this paper by "width of proton distribution" we will mean the inhomogeneous broadening, unless the opposite is specified explicitly.

For example, is was demonstrated by Murakhtina *et al*.[9] and further analyzed by Limbach *et al*.[29] that in HCl – water mixtures there is an extremely wide distribution of hydrogen bond geometries manifested as wide distribution of ^{1}H NMR chemical shifts, covering the range from 1 to 12 ppm at low HCl concentrations and stretching all the way down to 19 ppm at higher HCl concentrations. Similar broad distribution of geometries and chemical shifts was observed in LiI – water mixtures,[30] where authors characterized the structure and picosecond dynamics of the hydrogen bond network by means of first-principles molecular dynamics simulations at ambient temperature.

The ensemble of H-bond geometries is often sensitive to temperature and/or solvent polarity.[31] For example, in crystallography this can be manifested by the changed in the proton thermal displacement ellipsoids ("proton shape"[32-34]).[35] In hetero-conjugated anionic complexes of phenolate anions with carboxylic acids, an increase in solvent polarity shifts the bridging proton towards the phenolate moiety.[8]

There are several experimental techniques to study fluxional H-bonds in condensed phase. Apart of the neutron scattering[36] (also in liquid state[37]), these are fluorescence labeling,[38] terahertz,[39] and pump-probe IR,[40] as well as NMR[7, 41] spectroscopies. In recent years, using solid-state NMR in combination with crystallographic techniques, fairly good correlations were observed[2, 29, 42-47] for ^{1}H, ^{13}C, ^{15}N and ^{19}F NMR chemical shifts and H-bond geometry. NMR hydrogen bond correlations were successfully applied in studies of a large variety of systems, including self-associates of acids,[42] acid-base complexes,[21, 43, 48] functional H-bonds in cofactors,[49] and enzymes.[50] The continuous change of the NMR parameters upon continuous change of the H-bond geometry means that if there is a set of fast interchanging geometries then there is a set of NMR parameters, which is subsequently averaged out over the time of NMR experiment into single experimentally observed solvent- and temperature-dependent value.[8, 51, 52] In contrast, the characteristic time scale of optical spectroscopy is much shorter and spectral bands of individual isomers can be observed

independently[53] or as part of the overall inhomogeneously broadened band.[54, 55] Band positions in optical spectroscopy could also be correlated with the hydrogen bond geometry. Previously it has been done for OH/NH stretching,[56, 57] PyO vibrational bands of pyridine oxides,[58] ring modes of pyridines,[59, 60] carbonyl stretch of carboxylic acids[23, 24] and others. Recently, using an experimental setup for combined liquid-state NMR and UV-Vis measurements within the magnet of an NMR spectrometer Koeppe *et al*.[61] studied a series of strongly hydrogen bonded complexes of chloronitrophenols with carboxylic acid anions.[7] A correlation of the UV-vis absorption band position of 2-chloro-4-nitrophenol with the bridging proton position was proposed. It was shown that for strongest complexes there is proton tautomerism and it was argued that the width of the dual UV-vis absorption band reflects the width of the H-bond geometries distribution.[8]

From theoretical standpoint proton transfer reactions have long been a staple of various computational methods (see f.e. Ref. 62 and references cited therein) and more recently of *ab initio* molecular dynamics (AIMD) simulations.[63-68] Note, that in the literature the term AIMD is used alongside such terms as QM MD or DFT MD. In solution proton transfer can occur from a large variety of configurations, giving rise to different types of transient states, many of which have been anticipated within the context of the Grotthuss mechanism – for example Zundel or Eigen type cations.[69-71] In recent times also concerted proton transfer across several molecular centers has been proposed from such simulations.[72-74] These results illustrate the highly complex nature of the reaction coordinate manifold in solution.[75] On the one hand, empirical forcefield based molecular dynamics simulations usually have difficulties in describing the associated bond breaking processes in this context, though several approaches have been implemented over the last decade to lift this problem.[76-80] On the other hand, static quantum chemical calculations are not able to deal with the large number of possible transitions, hence the dominance of AIMD as a tool to investigate these processes. While the above applies mostly to aqueous solutions, model systems with well-defined proton exchange pathways serve a useful purpose in investigating proton transfer reactions.[81-83] In the past such systems have often been used to study nuclear quantum effects, *e.g.* proton quantum delocalization, which is substantial in systems with low barriers and at low temperatures.[84-88]

Following the research line started by some of us in Refs. [7, 8, 61] in this work we have chosen a complex formed by *para*-nitrophenol with tetraethylammonium (TEA) acetate dissolved in polar aprotic $CD_2Cl_2/CDCl_3$ mixture (Fig. 2). The phenol-acetate complexes could be considered as models systems for interactions between glutamic and aspartic acid side chains with tyrosine side chain or various cofactors, such as p-coumaric acid thioester in Photoactive Yellow Protein[89] or phenolic inhibitors of Ketosteroid Isomerase[90]. For the calculations we used tetramethylammonium (TMA) acetate and CD_2Cl_2 (DCM) as a solvent. We were interested in hydrogen bond geometry distribution, as well as spectroscopic parameters distribution, caused by interactions with complex's immediate surroundings, *i.e.* with solvent molecules and counterion in the solvation shell. The system has been studied experimentally by ^1H, ^{13}C NMR and UV-vis spectroscopy and theoretically by *ab initio* molecular dynamics and quantum-chemical calculations. In this study we focus on an oft neglected aspect in the study of proton transfer, which is the role of noncovalent interactions, especially due to solvent fluctuations. The role of solvent relaxation for charge and proton transfer is well known from Marcus-theory,[91-93] however to the best of our knowledge the role of dielectric solvation fluctuations for proton transfer reactions in anionic OHO-bonded complexes has not been investigated using full AIMD solvation yet.

The main questions for this work were as follows: (i) what are the primary solvent-solute interactions responsible for proton transfer? (ii) how does the distribution of H-bond geometries look like in solution, does two-state proton tautomerism model hold?

2. Experimental details

Low-temperature ^1H and ^{13}C NMR spectra were recorded in Center for Magnetic Resonance of St. Petersburg State University on a Bruker DPX-300 NMR spectrometer (working frequency 300.13 MHz for ^1H and 75.47 MHz for ^{13}C). Low-temperature NMR/UV-vis spectra were recorded by Dr. Benjamin Koeppe at Freie Universitaet Berlin on a Bruker AMX-500 NMR spectrometer (working frequency 500.03 MHz for ^1H) equipped with UVNMR probe which allows one to measure NMR and UV-vis spectra at the same time as described in Ref. [7]. NMR chemical shifts were measured using $CHDCl_2$ (CD_2Cl_2) as internal

standard and converted to the conventional TMS scale.

Sample preparation for NMR and UVNMR measurements. TEA ^{13}C-acetate was obtained by reaction of TEA hydroxide solution in methanol (Fluka) with 1-^{13}C-acetic acid (Cambridge Isotope) directly in NMR sample tube equipped with a J. Young valve; then the solvents were removed on a high vacuum line. After that 1-^{13}C-*para*-nitrophenol (obtained by cyclization[94] of 2-^{13}C-acetone with sodium nitromalonaldehyde[95]) and deuterated solvent was added. In order to deuterate the compounds in the mobile proton sites the NMR sample tube containing the already prepared sample was attached to a high-vacuum line, and the solvent was evaporated. After that about 0.2 mL of methanol-OD (99.5%; Euroisotope) was added to the sample and subsequently evaporated. Finally, the sample was again dissolved in deuterated solvent. ^{13}C enriched substances were used to shorten the experiment time and to lower the concentrations of the substances, which is beneficial if one wants to slow down molecular and proton exchange processes.

3. Computational details

We performed *ab initio* molecular dynamics simulation (AIMD or DFT MD) of the solvated complex using the CP2K[96] simulation package (CP2K is not an actual abbreviation, but tentatively it stands for Car-Parrinello code for the new millenium). We chose GPW (Gaussian Plane Wave)[97] method, the BLYP-D (Becke, Lee, Yang, Parr potential with Grimme dispersion corrections)[98-100] DFT (Density Functional Theory) functional together with a TZVP (Triple-Zeta Valence Polarized) basis on all atoms with the exception of oxygen and hydrogen, for which an aug-TZV2P / TZV2P basis sets were used, respectively. The planewave cutoff was set to 350 Ry. We used GTH (Goedecker, Teter and Hutter)[101] pseudopotentials for all atoms. The simulations were performed in an NVT ensemble (canonical ensemble with number of particles, temperature and volume as thermodynamic variables) at 300 K using a CSVR (Canonical Sampling through Velocity Rescaling)[102] thermostat with a time constant of 100 fs. All hydrogen atoms were simulated as deuterium atoms, which allowed us to increase the time step to 1 fs; from now on we will refer to them as “protons” for convenience. The employed SCF (Self-Consistent Field) convergence was 10^{-8} a.u. The molecular dynamics was done in a cubic periodic box with a side length of 20 Å. The initial geometry of the complex was

optimized in gas phase using Gaussian09.[103] Then the complex was inserted in previously equilibrated solvent box by calculating the molecular volume of the overlapping Van der Waals radii of its atoms and removing the equivalent volume of DCM molecules calculated in the same way. This resulted in a box containing the complex of *para*-nitrophenol with acetate anion and 71 DCM molecules at a density 1.3 g/cm^3. The system was pre-equilibrated for 16 ps using a TZVP basis set for all atoms, then the simulation continued for another 10 ps with an increased basis set for O and H. The last 10 ps were used for data sampling. To take into account counterion effects we did another simulation in the same setup with the TMA cation included into the previously equilibrated box containing the complex and 70 DCM molecules. In this case data were sampled for 24 ps after 5 ps of equilibration. TZV2P-GTH for hydrogen and aug-TZV2P-GTH for oxygen atoms were used throughthout the trajectory. We used VMD (Visual Molecular Dynamics)[104] and TRAVIS (TRajectory Analyzer and VISualizer)[105] for trajectory analysis.

Chemical shifts were calculated in Gaussian09 at PBE0/IGLO-III (Perdew, Burke and Ernzerhof / Individual Gauge for (each) Localized Molecular Orbital)[106-109] level of theory for 70 random snapshots extracted from the trajectory. All solvent molecules within 3.3 Å range from the complex were taken into account as well as the counter-cation. Isotropic magnetic shieldings were referenced to TMS (tetramethylsilane) calculated in Gaussian09 at the same level of theory.

4. Results

4.1 *Low-temperature ^{1}H, ^{13}C NMR and UVNMR experiments.* The ^{1}H and ^{13}C NMR spectra of the sample containing partially deuterated 1-^{13}C-*para*-nitrophenol (0.75 mM) and TEA 1-^{13}C-acetate (1.5 mM) dissolved in a 5:1 CD_2Cl_2:$CDCl_3$ mixture at 173 K were measured. Parts of these spectra are presented in Fig. 3a, assignment of the signals was done according to Ref. [7]. At 173 K the slow exchange regime is reached allowing us to detect various intermolecular complexes. In Fig. 3a the homo-conjugated complexes of phenol and acetic acid are labeled PLP and ALA (L = H, D), respectively, and the hetero-conjugated complex's signals are marked with H and D.

The ^{1}H NMR chemical shift of the bridging proton of the hetero-conjugate equals 17.5 ppm; it

means that the strong and short H-bond is formed in the complex. As the sample was partially deuterated at the bridging proton site, we were able to resolve the H/D isotope effect on ^{13}C chemical shift of *ipso*-phenolic carbon $\Delta(H/D) = \delta[C(D)] - \delta[C(H)] = -1.4$ ppm. The isotope effect on the carboxylic carbon chemical shift was not resolved but from the line shape of the signal it was estimated to be not larger than 0.15 ppm by the absolute value.

The low-temperature UV-vis spectrum of the sample containing non-deuterated *para*-nitrophenol with TEA acetate dissolved in CD_2Cl_2 measured at 180 K is shown in Fig. 3b. The absorption band is assigned to the hetero-conjugated complex because the sample preparation procedure ensured that this is the only complex with *para*-nitrophenol in the solution (see Ref. [7,8] for more details). The simultaneously measured bridging proton chemical shift of the hetero-conjugated complex for this sample coincided with that shown in Fig. 3a.

4.2 *Ab initio molecular dynamics calculations*.

We ran two trajectories: for the solvated anionic complex without the counterion, as well as for the solvated anionic complex with the counterion (tetramethylammonium, TMA). Along the trajectory without the counterion the complex is stable and the hydrogen bond does not break, the non-planar *trans*-form of the complex dominates (see schemes in Fig. 4); terms *cis* and *trans* refer to the relative positions of C=O and phenyl with respect to the H-bond. For the trajectory with the counterion the situation is similar: there is stable non-planar complex mostly in a *trans*-form. The contact ion pair is not broken by the solvent molecules.

Throughout the paper, in order to represent the hydrogen bond geometry we have selected linear combinations of interatomic distances $q_1 = ½ (r(\text{PhO…H}) - r(\text{H…OAc}))$ and $q_2 = (r(\text{PhO…H}) + r(\text{H…OAc}))$. For a linear hydrogen bond the physical meaning of these parameters is as follows: q_1 represents the displacement of the bridging proton from the hydrogen bond center, while q_2 stands for the overall hydrogen bridge length.[110, 111] Alternatively, we could have stayed with r(PhO...H) and r(PhO...OAc) distances as main geometric parameters, but this could be disadvantageous in some respects. The difference between q_2 and r(PhO...OAc) becomes more apparent for non-linear H-bonds. There, O...O distance contains less information about the proton position than q_2. For this reason and because the q_2 parameter as a natural pair to the H-bond asymmetry parameter q_1 has been

extensively used previously for the analysis of OHO hydrogen bonds,[29, 42, 110] we chose to use it in the manuscript. In both cases, with and without the counter-cation, the bridging proton crosses H-bond center several times during the simulation (Fig. 4).

5. Discussion.

5.1 *Experimental data*. The chemical shift of the bridging proton of 17.5 ppm corresponds to an asymmetric strong and short hydrogen bond (Fig. 3a).[29] From this value alone it is hard to tell which geometry of the complex dominates in the solution, of type PhOH···$^{-}$OAc or of type PhO^{-}···HOAc. To overcome this problem the complex was partially deuterated in the mobile proton site, which allowed us to measure the H/D isotope effect on ^{13}C chemical shift of *ipso*-phenolic carbon. According to Ref. [7], the negative sign of the measured isotope effect corresponds to the situation when average proton position is shifted towards phenolic group. The opposite sign of isotope effect would be characteristic for dominating PhO^{-}···HOAc structures. In our case isotope effect is –1.14 ppm, clearly indicating that PhOH···$^{-}$OAc type of structures dominate in the solution. One should keep in mind that observed NMR parameters are averaged over the processes which are fast in NMR time scale and proton motion, including proton tautomerism, is definitely among such processes. Thus, the information concerning the distribution of hydrogen bond geometries in solution is to a big extent "washed out" from NMR spectra. In contrast to NMR, the characteristic time of UV-vis spectroscopy is much shorter and bands in UV-vis spectra are often inhomogeneously broadened, reflecting the distribution of structures in solution. Following the methodology proposed in Ref. [7] here we deconvolute the absorption band in UV-vis spectrum into two bands of lognormal shape, see dashed vertical lines in Fig. 3b. Centers of gravity for those bands are at 340 nm and 390 nm. These wavelengths are common for absorption of *para*-nitrophenol and *para*-nitrophenolate anion involved in H-bond formation, respectively. It could be concluded that two forms of *para*-nitrophenol exist in the solution and correspond to two strongly H-bonded proton tautomers of the complex: PhOH···$^{-}$OAc and PhO^{-}···HOAc. Extinction coefficient of nitrophenolate anion is a bit larger than that of the nitrophenol,[112] so relying on integral intensities of these bands we can say that the PhOH···$^{-}$OAc form of the complex dominates, in agreement with NMR results.

A couple of remarks has to be done concerning the deconvolution procedure of UV-vis spectrum shown in Fig. 3b. Firstly, the absence of sharp spectral features at the first glance masks the presence of two bands (the situation which is not at all rare in UV-Vis spectroscopy). However, the studied complex is just one of the examples in a larger series of

similar complexes (see Ref. [7, 8] and supporting information for these papers), for many of which the band separation is more pronounced and for all of which the deconvolution into two bands worked very well. Band positions and relative band intensities lie in a series of values obtained for similar complexes of *para*-nitrophenol, which increases the reliability of our deconvolution. Finally, in terms of our original idea of detecting the presence of a whole ensemble of "solvatomers", the deconvolution into two bands only might be considered insufficient. We think that this argument is a perfectly valid one, though the quality of the fit obtained using only two bands was good enough and we saw no necessity to go beyond it.

Summarizing the experimental findings so far we conclude that a) the studied complex has short and strong hydrogen bond, b) broad UV-vis absorption band could be deconvoluted into two bands corresponding to PhOH···$^-$OAc and PhO$^-$···HOAc forms of the complex and c) PhOH···$^-$OAc form dominates.

5.2 *Ab initio MD data*. Now we turn to the analysis and discussion of the results of MD simulations. We will focus mostly on the hetero-conjugated complex with counter-cation, while the complex without cation will be mentioned briefly where applicable. In Fig. 5 we show the view of typical structure of the solute in the MD simulation. This is *trans*-form of the complex with counter-cation located in the vicinity of the hydrogen bridge.

Due to constant changes of the complex's structure it is better to describe it in terms of distributions of several key geometric parameters. Dihedral angle γ_1(COOO) describes how planar is the complex: γ_1 = 0° stands for planar *cis*-complex, γ_1 = 180° means planar *trans*-complex (Fig. 6a); by planar we mean that phenyl ring and carboxylic group are in one plane. Distribution of γ_1 has its maximum close to 140° and it is broad, meaning that it is a *trans*-structure which is non-planar on average, though sometimes it reaches planarity during the simulation.

The H-bond stays almost linear along the trajectory (Fig. 6b) and it lies along the lone pair of the oxygen atom of phenol and perpendicular to the O-O line connecting two oxygen atoms of the acid (Fig. 6c and d).

The H-bond geometry changes a lot during the simulation, however, it is never broken and q_2 as a function of q_1 during the simulation has expected shape (Fig. 7, left).[29] For the structures with quasi-symmetric H-bonds (small q_1 values) the difference between q_2 and r(PhO...OAc)

distances becomes negligible, because the OHO angle for such structures is close to 180 degrees and one may state that quasi-symmetric H-bonds also correspond to shortest distances between oxygen atoms. In contrast, when O...O distance becomes larger, the deviation from linearity could be more significant and in this case q_2 would be the preferred parameter to describe the H-bond geometry. The overall proton position distribution is plotted versus q_1 distance in Fig. 7, right. The obtained distribution is very broad; it covers the range from quasi-symmetric H-bonds to highly asymmetric H-bonds; structures interconvert due to the solvent motions. For the trajectory with TMA there are two broad maxima of almost equal intensity corresponding roughly to the $PhO^{-}\cdots HOAc$ and $PhOH\cdots{}^{-}OAc$ forms, which can be interpreted as two proton tautomers represented by many individual structures each. Distribution of proton position differs significantly for the case with and without counter-cation (black triangles and red circles in Fig. 7, right, respectively). For the case without TMA $PhO^{-}\cdots HOAc$ form dominates in the solution. Note that there is a significant difference between the experimental and simulated temperatures (T = 180 K versus T = 300 K). The increased simulation temperature was chosen in view of enhancing the phase space sampling during the molecular dynamics simulations. The main consequence of this higher temperature is a faster transition between local conformational minima, yielding a much higher numerical efficiency. Previously published experimental observations[8] indicate that a lowered simulation temperature shifts the proton distribution in the hydrogen bond towards the PhOH...-OAc form, corresponding to a preferential stabilization of a more compact charge.

Autocorrelation function for q_1 along the trajectory with TMA is shown in Fig. 8. Correlation time for proton motion is $\tau_c = 0.72$ ps. τ_c could be interpreted as life-time of one proton tautomer and this characteristic time is close to the rotational correlation time of DCM at 300 K.[15-19]

The question arises which dynamic process induces proton displacement between two groups of solvatomers (two tautomers, in short)? In other words, what should change in the solvation shell for the bridging proton to jump? As the structure of the solvation shell is rather complicated, in order to tackle these questions we have analyzed a number of geometric parameters of the solvation shell looking for the key elements. Below we present analysis of

only those parameters, which proved to be indicative for the hydrogen bond geometry. These parameters are: angle β(OON) formed by two oxygen atoms of acetic acid and nitrogen atom of TMA (Fig. 9, left), as well as radial distribution functions between oxygen atom of "free" carbonyl and protons of DCM molecules (Fig. 9, right). What do these parameters mean?

A correlation between angle β and q_1 (Fig. 9, left) exhibits distinct asymmetry in positions of probability maxima. For $PhO^{-}\cdots HOAc$ forms average angle β is somewhat larger and representative structure of the complex is shown in the left part of Fig. 10. For $PhOH\cdots{}^{-}OAc$ the average β is smaller and the corresponding structure is presented in the right part of Fig. 10. This finding will be interpreted in next paragraphs.

Radial distribution functions between oxygen atom of "free" carbonyl and protons of DCM for the trajectory with counter-cation and without it differ a lot at short distances (Fig. 9, right, black and green solid lines, respectively). It looks like for the trajectory with TMA DCM molecules come closer to "free" carbonyl. We have subdivided the trajectory with TMA into two parts relative to q_1 sign and built radial distribution functions for them separately (Fig. 9, right, red and blue dashed lines). For the $PhOH\cdots{}^{-}OAc$ form ($q_1 > 0$) there are more protons of DCM molecules at shorter distances than for $PhO^{-}\cdots HOAc$ ($q_1 < 0$) form. Apparently, there is an interaction between CH protons of DCM and oxygen atom of "free" carbonyl of acetic acid. To look at the nature of this interaction we have built a correlation between distance r_1 from oxygen atom of "free" carbonyl to DCM protons and CHO angle ϕ_1 (see Fig. 11). This two-dimensional correlation has its maximum close to linear bond ca. 2.2 Å long (Fig. 11a), which means that a weak H-bond is formed between "free" carbonyl and DCM. And for the $PhOH\cdots{}^{-}OAc$ form this bond is more linear and shorter than for the $PhO^{-}\cdots HOAc$ form (Fig. 11b and c, respectively).

Now we can put together and rationalize findings of Figures 9 and 11. On the one hand, when "free" carbonyl points towards TMA the CH···O bond with the solvent is somewhat disrupted. On the other hand, when "free" carbonyl is turned aside there is enough space for DCM molecules to come closer and form a stronger H-bond. In other words, for the complex of *para*-nitrophenol with acetate anion it is the relative motion of TMA and "free" carbonyl that plays the major role in the OHO bond geometry changes and proton jumps. Weak H-bonds between DCM protons and oxygen atom of "free" carbonyl stabilize $PhOH\cdots{}^{-}OAc$ type of

structures.

5.3 *Quantum-chemical calculatios of NMR parameters*. To be able to compare experimental results with the results of *ab initio* MD simulations we have calculated NMR chemical shifts of the bridging proton. δH as a function of q_1 is shown in Fig. 12; this dependence has expected shape reaching its maximum for the central-symmetric bonds. Average value is 18.3 ppm which is in a reasonably good agreement with the experimental value 17.5 ppm. Note, however, that this average value is the result of averaging over a rather wide range of values, ca. 14 – 23 ppm, reflecting the ensemble of structures interconverting in solution. At this point it is not clear what causes δH values as high as 23 ppm for quasi-symmetric H-bonds. It might be a combination of ring current effects in phenyl ring and intermolecular contributions from surrounding DCM molecules.

6. Conclusions

We have investigated intermolecular complex with strong OHO hydrogen bond in solution: anionic complex of *para*-nitrophenol with tetraalkylammonium acetate in DCM. The system was studied experimentally and theoretically. Low-temperature ^{1}H, ^{13}C NMR and UV-vis spectra show that strong and short H-bond is formed with a wide distribution of H-bond geometries in the solution. This distribution could be divided into PhOH···$^{-}$OAc and PhOH···$^{-}$OAc structures that interconvert to one another under the influence of solvent thermal fluctuations. With *ab initio* MD simulations we were able to look at solvent-solute interactions as well as their development in time in atomistic detail. We show that this is the relative motion of TMA and "free" carbonyl that plays the major role in the OHO bond geometry changes and proton jumps. Weak H-bonds between DCM protons and oxygen atom of "free" carbonyl stabilize PhOH···$^{-}$OAc type of structures, while "blocking" of C=O group by counter-cation disrupts CH···O bonds and favors PhOH···$^{-}$OAc structures. We have tried to visualize this schematically in Fig. 13. In other words, the partial electron transfer accompanying the formation of weak C-H···O=C bond decreases the proton accepting ability of the other oxygen atom of the acetate and subsequently depopulates PhO^{-}···HOAc structures. In the future it would be interesting to see how these conclusions will change for a neutral system having no counter-cation, for example, for a neutral OHN bonded complex.

Acknowledgement

We thank the German-Russian Interdisciplinary Science Center (G-RISC) funded by the German Federal Foreign Office via the German Academic Exchange Service (DAAD) and the Russian Foundation of Basic Research (Projects 14-03-00111 and 14-03-00716) for financial support.

Figures and captures

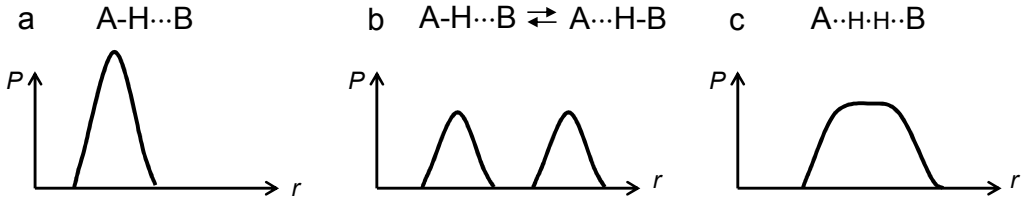

Figure 1. Schematic representation of the hypothetical proton probability distribution function (P) of a H-bonded complex AHB versus the proton transfer coordinate r in three cases: (a) a narrow distribution of geometries approximated by a single structure, (b) two groups of structures represented by two proton tautomers and (c) a broad distribution of geometries.

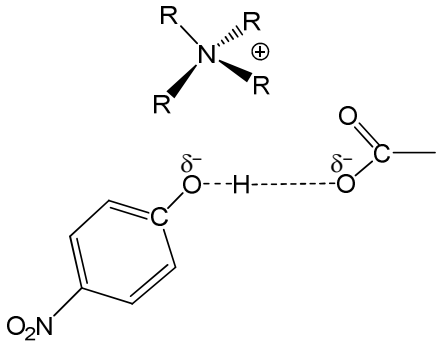

Figure 2. Complex of *para*-nitrophenol with tetraalkylammonium acetate. R was ethyl for experimental part and methyl for calculations. Proton position within H-bond is chosen arbitrarily.

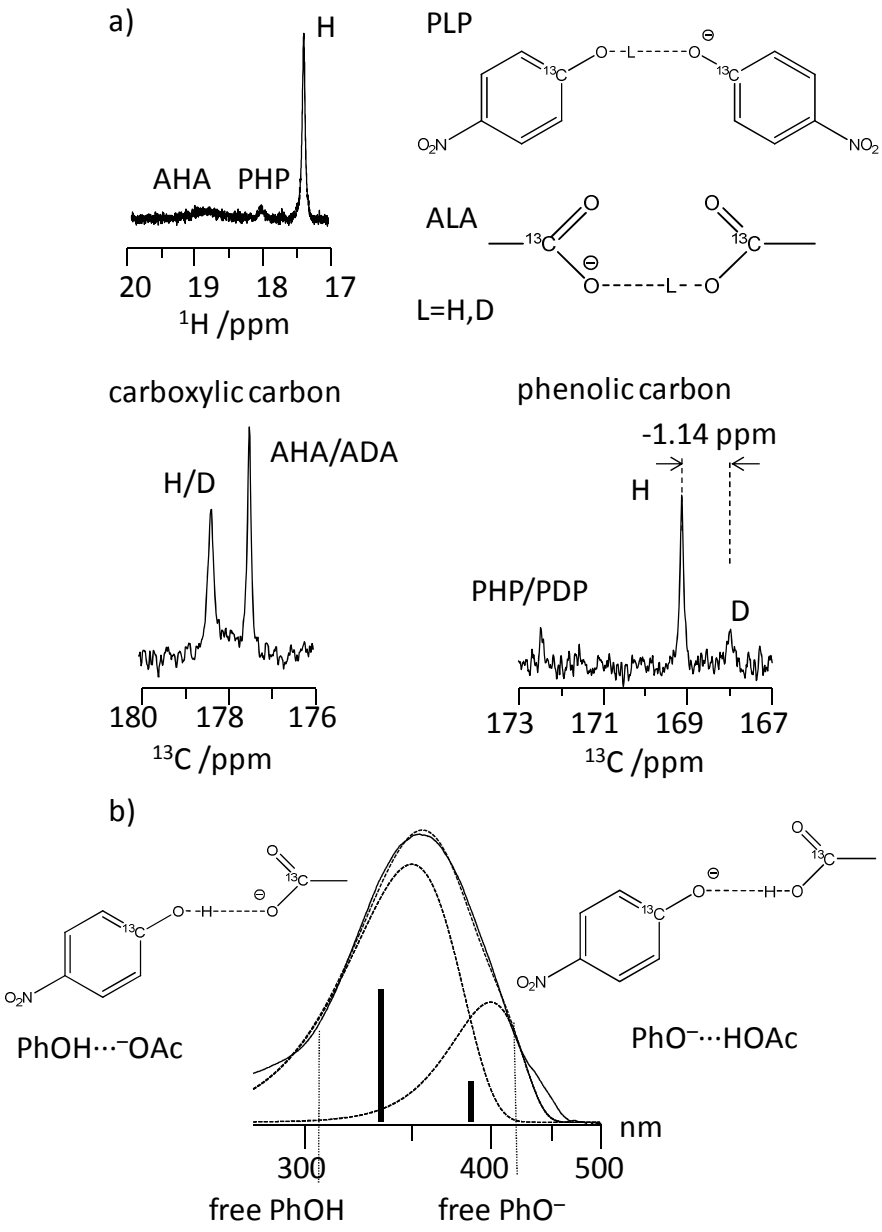

Figure 3. a) Parts of ^{1}H and ^{13}C NMR spectra of the sample containing partially deuterated 1-^{13}C-*para*-nitrophenol and TEA 1-^{13}C-acetate dissolved in 5:1 CD_2Cl_2:$CDCl_3$ mixture and measured at 173 K; signals of the non-deuterated and deuterated forms of the hetero-conjugated complex are marked with H and D respectively, other signals belong to homo-conjugated anions of acid and phenol (ALA and PLP, respectively, L = H, D); b) UV-vis spectrum of the H-bonded complex between *para*-nitrophenol and TEA acetate measured at 180 K in CD_2Cl_2.

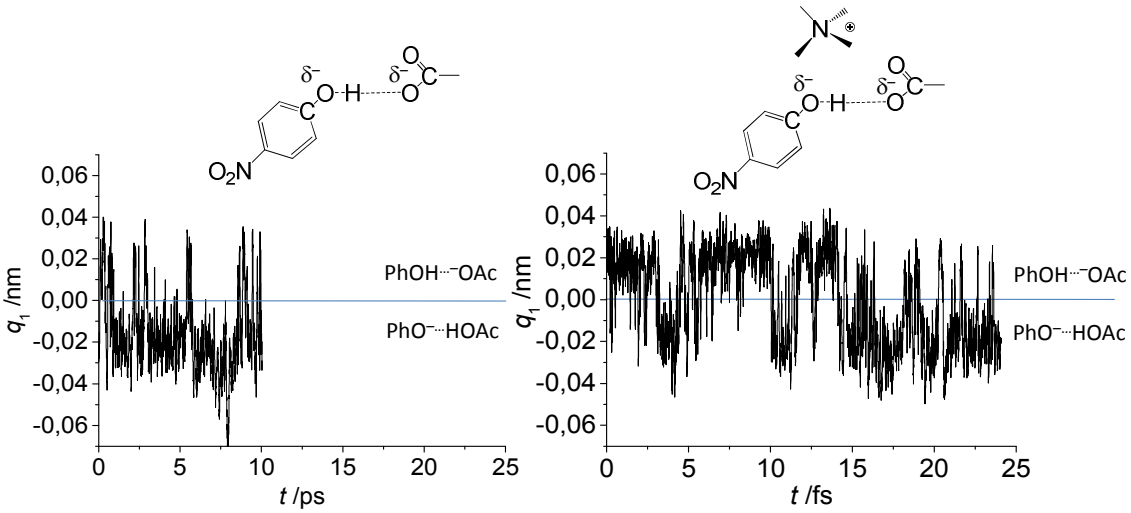

Figure 4. Evolution of $q_1 = ½ (r(\text{PhO}\ldots\text{H}) - r(\text{H}\ldots\text{OAc}))$ with time during simulation of nitrophenol-acetate complex with TMA as counter-cation (right) and without it (left).

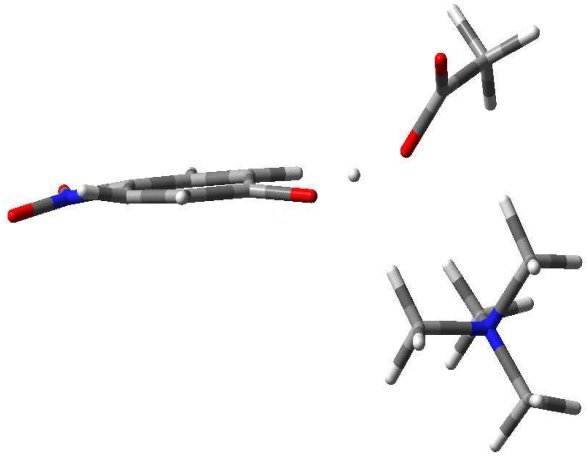

Figure 5. Snapshot of the trajectory with the complex and TMA in solution (DCM molecules were removed for clarity).

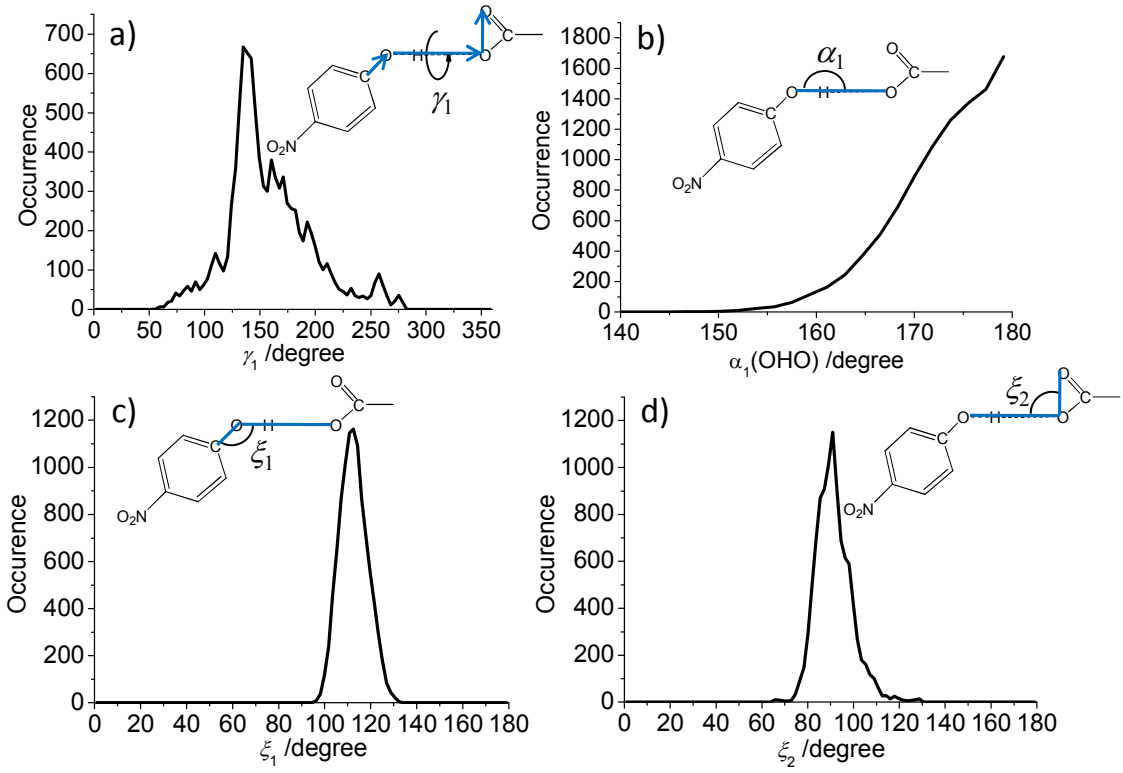

Figure 6. Distribution of γ_1, α_1, ξ_1 and ξ_2 during data sampling. Definitions of geometric parameters are given in the schemes included into each plot.

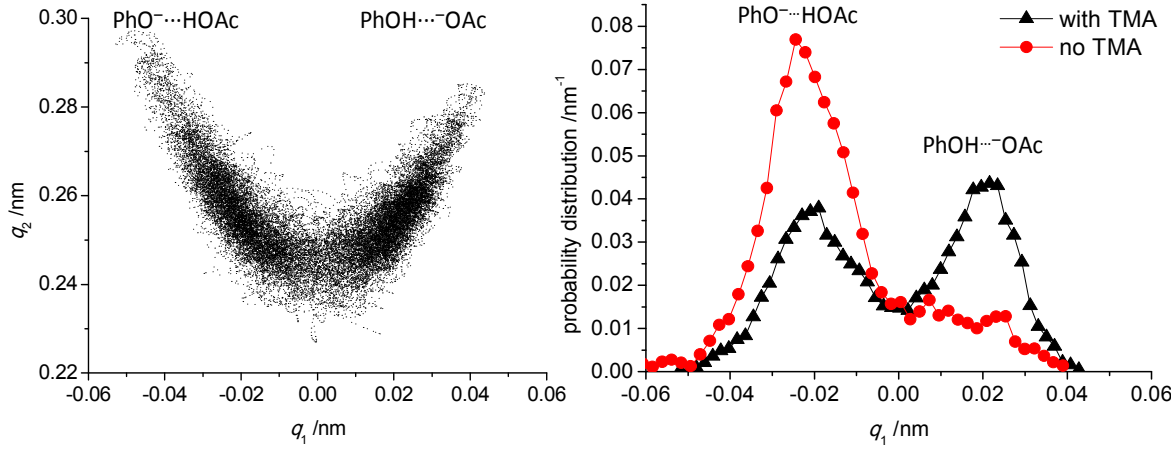

Figure 7. Left: $q_2 = r$(PhO…H) + r(H…OAc) as a function of $q_1 = ½$ (r(PhO…H) – r(H…OAc)) during the simulation with TMA. Right: q_1 distribution for the trajectory with TMA (black triangles) and without TMA (red circles).

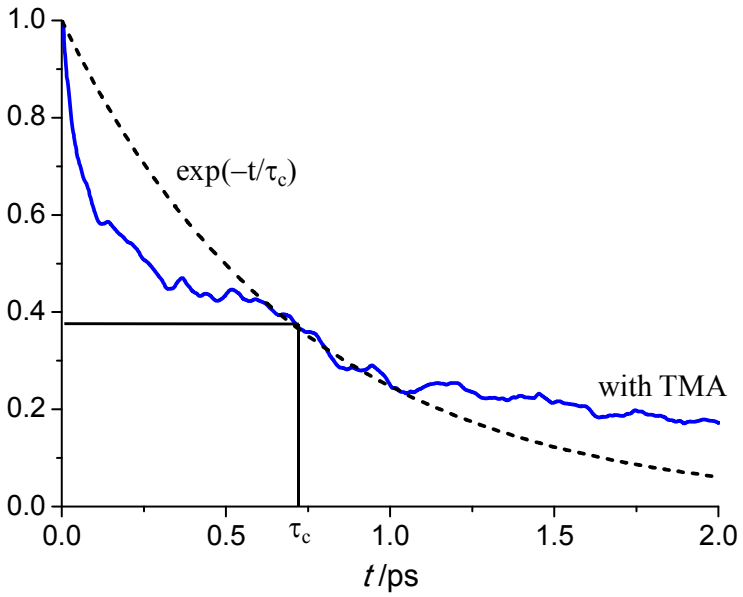

Figure 8. Autocorrelation function for bridging proton motion in the *para*-nitrophenol complex with acetate anion with TMA. Correlation time is 0.72 ps. Dash-dotted line is least squares exponential fit.

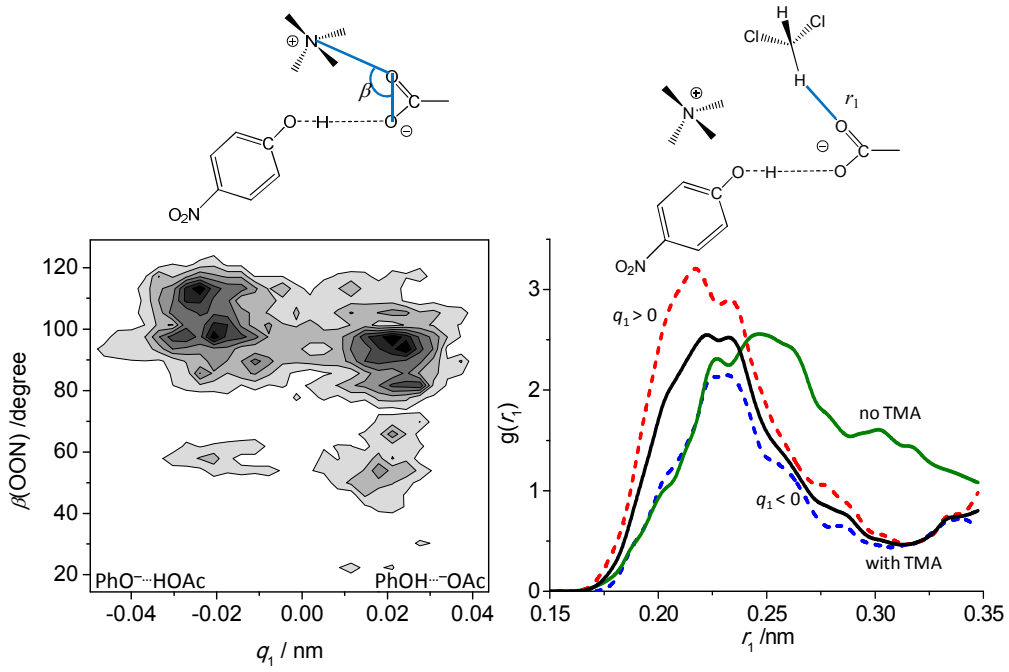

Figure 9. Left: two-dimensional correlation between q_1 and angle β (defined as shown in the scheme); darker colours correspond to higher intensity. Right: radial distribution functions for oxygen atom of "free" carbonyl to protons of DCM molecules. Green for the trajectory without TMA. Black for the trajectory with TMA, which is an average of two parts: red dashed line for PhOH···$^-$OAc forms ($q_1 > 0$) and blue dashed line for PhO$^-$···HOAc forms ($q_1 < 0$).

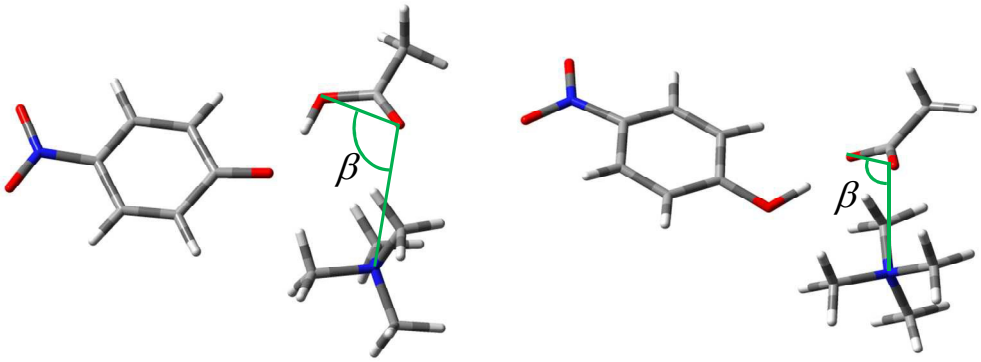

Figure 10. Representative structures of the complex with large (left) and small (right) value of β(OON).

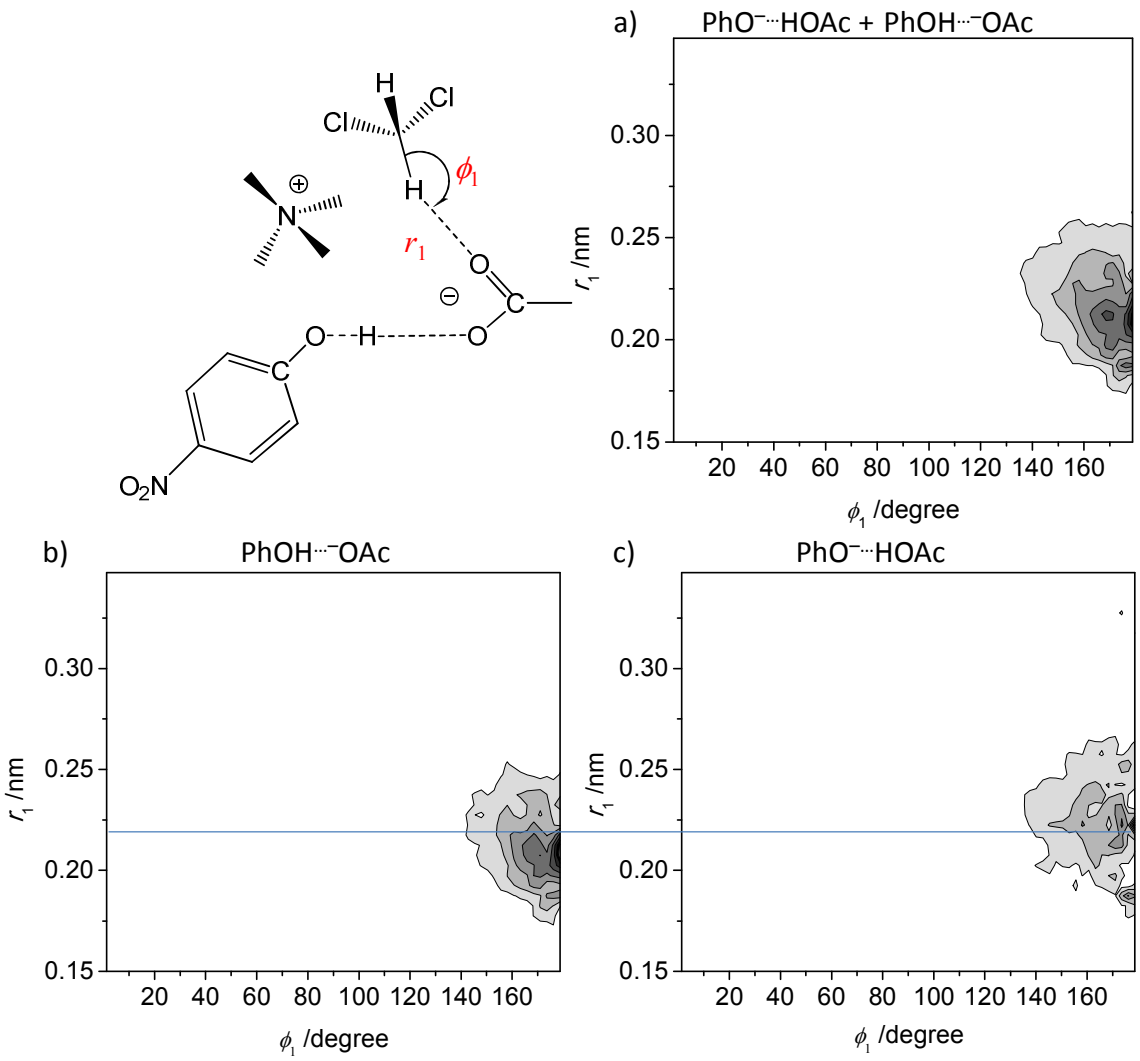

Figure 11. Correlation between distance r_1 from oxygen atom of "free" carbonyl to DCM protons and CHO angle ϕ_1 for the trajectory with TMA (a) and its subdivision into two parts for $q_1 < 0$ (b) and $q_1 > 0$ (c). Blue line is a guide for an eye. Darker colours correspond to higher intensity.

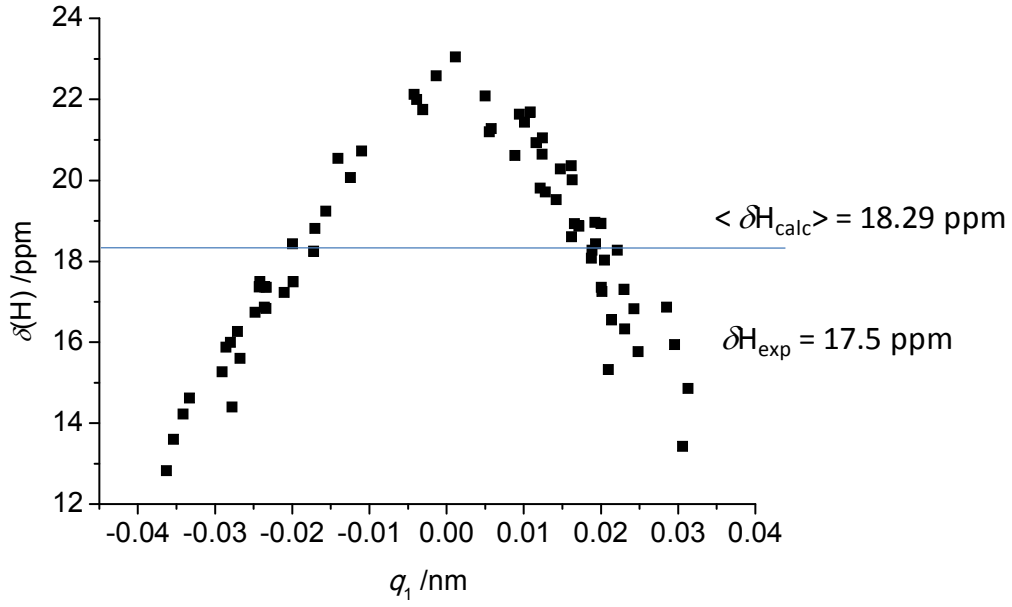

Figure 12. Calculated δH as a function of q_1 for OHO^- system.

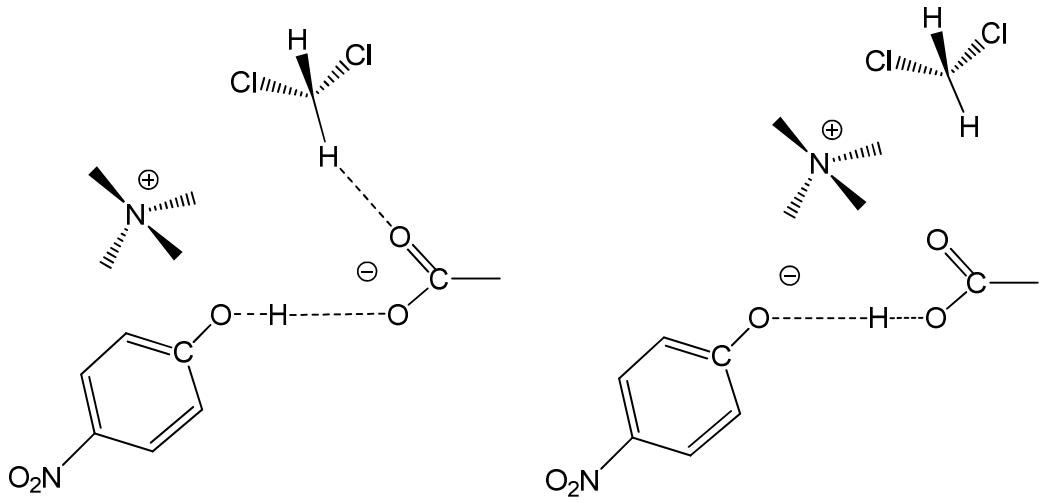

Figure 13. Schematic representation of PhOH···$^-$OAc and PhOH···$^-$OAc structures with relative positions of counter-cation and solvent molecule.

References

1. J. E. Del Bene and M. J. T. Jordan, *J. Phys. Chem. A*, 2002, **106**, 5385-5392.
2. P. Lorente, I. G. Shenderovich, N. S. Golubev, G. S. Denisov, G. Buntkowsky and H.-H. Limbach, *Magn. Reson. Chem.*, 2001, **39**, S18-S29.
3. M. Mikami and S. Nakamura, *Phys. Rev. B*, 2004, **69**, 134205.
4. E. L. Mertz and L. I. Krishtalik, *Proc. Natl. Acad. Sci. U. S. A.*, 2000, **97**, 2081-2086.
5. L. Sobczyk, *Appl. Magn. Reson.*, 2000, **18**, 47-61.
6. R. D. Bach, O. Dmitrenko and M. N. Glukhovtsev, *J. Am. Chem. Soc.*, 2001, **123**, 7134-7145.
7. B. Koeppe, P. M. Tolstoy and H.-H. Limbach, *J. Am. Chem. Soc.*, 2011, **133**, 7897-7908.
8. B. Koeppe, J. Guo, P. M. Tolstoy, G. S. Denisov and H.-H. Limbach, *J. Am. Chem. Soc.*, 2013, **135**, 7553-7566.
9. T. Murakhtina, J. Heuft, E. J. Meijer and D. Sebastiani, *ChemPhysChem*, 2006, **7**, 2578-2584.
10. C. L. Perrin, *Pure Appl. Chem.*, 2009, **81**, 571-583.
11. C. L. Perrin and J. S. Lau, *J. Am. Chem. Soc.*, 2006, **128**, 11820-11824.
12. V. K. Yadav and A. Chandra, *J. Chem. Phys.*, 2013, **138**, 224501.
13. S. A. Kirillov, M. I. Gorobets, M. M. Gafurov, M. B. Ataev and K. S. Rabadanov, *J. Phys. Chem. B*, 2013, **117**, 9439-9448.
14. J. Zheng, K. Kwak, J. Asbury, X. Chen, I. R. Piletic and M. D. Fayer, *Science*, 2005, **309**, 1338-1343.
15. A. Hacura, *J. Mol. Liq.*, 1992, **54**, 33-38.
16. H. S. Sandhu, *J. Magn. Reson.*, 1978, **29**, 563-572.
17. J. Hunger, A. Stoppa, A. Thoman, M. Walther and R. Buchner, *Chem. Phys. Lett.*, 2009, **471**, 85-91.
18. D. E. O'Reilly, E. M. Peterson and E. L. Yasaitis, *J. Chem. Phys.*, 1972, **57**, 890-894.
19. T. Fox and P. A. Kollman, *J. Phys. Chem. B*, 1998, **102**, 8070-8079.
20. Z. Dega-Szafran, M. Grundwald-Wyspiańska and M. Szafran, *Spectrochim. Acta, Part A*, 1991, **47**, 125-131.
21. P. Schah-Mohammedi, I. G. Shenderovich, C. Detering, H.-H. Limbach, P. M. Tolstoy, S. N. Smirnov, G. S. Denisov and N. S. Golubev, *J. Am. Chem. Soc.*, 2000, **122**, 12878-12879.
22. C. L. Perrin, J. S. Lau and B. K. Ohta, *Pol. J. Chem.*, 2003, **77**, 1693-1702.
23. G. M. Barrow, *J. Am. Chem. Soc.*, 1956, **78**, 5802-5806.
24. G. S. Denisov, J. Starosta and V. M. Schreiber, *Opt. Spectrosc.*, 1973, **35**, 447-452.
25. N. S. Golubev, G. S. Denisov and A. I. Koltsov, *J. Mol. Struct.*, 1981, **75**, 333-337.
26. J. Nasielski and E. V. Donckt, *Spectrochim. Acta*, 1963, **19**, 1989-2009.
27. N. S. Golubev, G. S. Denisov, S. N. Smirnov, D. N. Shchepkin and H. H. Limbach, *Z. Phys. Chem.*, 1996, **196**, 73-84.
28. M. Garcia-Viloca, À. González-Lafont and J. M. Lluch, *J. Am. Chem. Soc.*,

1999, **121**, 9198-9207.
29. H.-H. Limbach, P. M. Tolstoy, N. Pérez-Hernández, J. Guo, I. G. Shenderovich and G. S. Denisov, *Isr. J. Chem.*, 2009, **49**, 199-216.
30. C. Allolio, N. Salas-Illanes, Y. S. Desmukh, M. R. Hansen and D. Sebastiani, *J. Phys. Chem. B*, 2013, **117**, 9939-9946.
31. A. J. Barnes, Z. Latajka and M. Biczysko, *J. Mol. Struct.*, 2002, **614**, 11-21.
32. M. Benoit and D. Marx, *ChemPhysChem*, 2005, **6**, 1738-1741.
33. D. Marx, *ChemPhysChem*, 2006, **7**, 1848-1870.
34. D. Marx, *ChemPhysChem*, 2007, **8**, 209-210.
35. T. Steiner, I. Majerz and C. C. Wilson, *Angew. Chem., Int. Ed.*, 2001, **40**, 2651-2654.
36. T. Steiner and W. Saenger, *Acta Crystallogr., Sect. B*, 1994, **50**, 348-357.
37. A. K. Soper, *Chem. Phys.*, 2000, **258**, 121-137.
38. A. Dallmann, M. Pfaffe, C. Mügge, R. Mahrwald, S. A. Kovalenko and N. P. Ernsting, *J. Phys. Chem. B*, 2009, **113**, 15619-15628.
39. S. Ebbinghaus, S. J. Kim, M. Heyden, X. Yu, M. Gruebele, D. M. Leitner and M. Havenith, *J. Am. Chem. Soc.*, 2008, **130**, 2374-2375.
40. N. Huse, S. Ashihara, E. T. J. Nibbering and T. Elsaesser, *Chem. Phys. Lett.*, 2005, **404**, 389-393.
41. V. I. Chizhik, I. S. Podkorytov, A. P. Kaikkonen and V. I. Mikhailov, *J. Magn. Reson., Ser. A*, 1996, **123**, 1-6.
42. P. M. Tolstoy, P. Schah-Mohammedi, S. N. Smirnov, N. S. Golubev, G. S. Denisov and H.-H. Limbach, *J. Am. Chem. Soc.*, 2004, **126**, 5621-5634.
43. I. G. Shenderovich, P. M. Tolstoy, N. S. Golubev, S. N. Smirnov, G. S. Denisov and H.-H. Limbach, *J. Am. Chem. Soc.*, 2003, **125**, 11710-11720.
44. M. Pietrzak, J. P. Wehling, S. Kong, P. M. Tolstoy, I. G. Shenderovich, C. López, R. M. Claramunt, J. Elguero, G. S. Denisov and H.-H. Limbach, *Chem. - Eur. J.*, 2010, **16**, 1679-1690.
45. E. Brunner and U. Sternberg, *Prog. Nucl. Magn. Reson. Spectrosc.*, 1998, **32**, 21-57.
46. T. K. Harris and A. S. Mildvan, *Proteins: Struct., Funct., Bioinf.*, 1999, **35**, 275-282.
47. A. McDermott and C. F. Ridenour, in *eMagRes*, John Wiley & Sons, Ltd2007.
48. P. M. Tolstoy, S. N. Smirnov, I. G. Shenderovich, N. S. Golubev, G. S. Denisov and H.-H. Limbach, *J. Mol. Struct.*, 2004, **700**, 19-27.
49. S. Sharif, M. C. Huot, P. M. Tolstoy, M. D. Toney, K. H. M. Jonsson and H.-H. Limbach, *J. Phys. Chem. B*, 2007, **111**, 3869-3876.
50. S. Sharif, E. Fogle, M. D. Toney, G. S. Denisov, I. G. Shenderovich, G. Buntkowsky, P. M. Tolstoy, M. C. Huot and H.-H. Limbach, *J. Am. Chem. Soc.*, 2007, **129**, 9558-9559.
51. I. G. Shenderovich, A. P. Burtsev, G. S. Denisov, N. S. Golubev and H.-H. Limbach, *Magn. Reson. Chem.*, 2001, **39**, S91-S99.
52. N. S. Golubev, I. G. Shenderovich, P. M. Tolstoy and D. N. Shchepkin, *J. Mol. Struct.*, 2004, **697**, 9-15.
53. T. Scharge, T. N. Wassermann and M. A. Suhm, *Z. Phys. Chem.*, 2008, **222**,

1407.
54. L. O. Paulson and D. T. Anderson, *J. Phys. Chem. A*, 2009, **113**, 1770-1778.
55. T. Yamashita and K. Takatsuka, *J. Chem. Phys.*, 2007, **126**, -.
56. A. Novak, in *Large Molecules*, Springer Berlin Heidelberg1974, vol. 18, ch. 4, pp. 177-216.
57. W. Mikenda, *J. Mol. Struct.*, 1986, **147**, 1-15.
58. V. Balevicius, K. Aidas, I. Svoboda and H. Fuess, *J. Phys. Chem. A*, 2012, **116**, 8753-8761.
59. V. Balevicius, R. Bariseviciute, K. Aidas, I. Svoboda, H. Ehrenberg and H. Fuess, *Phys. Chem. Chem. Phys.*, 2007, **9**, 3181-3189.
60. S. M. Melikova, K. S. Rutkowski, A. A. Gurinov, G. S. Denisov, M. Rospenk and I. G. Shenderovich, *J. Mol. Struct.*, 2012, **1018**, 39-44.
61. P. M. Tolstoy, B. Koeppe, G. S. Denisov and H.-H. Limbach, *Angew. Chem., Int. Ed.*, 2009, **48**, 5745-5747.
62. A. Staib, D. Borgis and J. T. Hynes, *J. Chem. Phys.*, 1995, **102**, 2487-2505.
63. U. W. Schmitt and G. A. Voth, *J. Chem. Phys.*, 1999, **111**, 9361-9381.
64. M. Tuckerman, K. Laasonen, M. Sprik and M. Parrinello, *J. Chem. Phys.*, 1995, **103**, 150-161.
65. C. Lao-ngam, P. Asawakun, S. Wannarat and K. Sagarik, *Phys. Chem. Chem. Phys.*, 2011, **13**, 4562-4575.
66. L. Vilčiauskas, M. E. Tuckerman, G. Bester, S. J. Paddison and K.-D. Kreuer, *Nat. Chem.*, 2012, **4**, 461-466.
67. D. Marx, M. E. Tuckerman, J. Hutter and M. Parrinello, *Nature*, 1999, **397**, 601-604.
68. J. A. Morrone and M. E. Tuckerman, *J. Chem. Phys.*, 2002, **117**, 4403-4413.
69. B. F. Habenicht, S. J. Paddison and M. E. Tuckerman, *Phys. Chem. Chem. Phys.*, 2010, **12**, 8728-8732.
70. G. A. Ludueña, T. D. Kühne and D. Sebastiani, *Chem. Mater.*, 2011, **23**, 1424-1429.
71. O. Markovitch, H. Chen, S. Izvekov, F. Paesani, G. A. Voth and N. Agmon, *J. Phys. Chem. B*, 2008, **112**, 9456-9466.
72. A. Hassanali, M. K. Prakash, H. Eshet and M. Parrinello, *Proc. Natl. Acad. Sci. U. S. A.*, 2011, **108**, 20410-20415.
73. B. K. Mai, K. Park, M. P. T. Duong and Y. Kim, *J. Phys. Chem. B*, 2012, **117**, 307-315.
74. A. Hassanali, F. Giberti, J. Cuny, T. D. Kühne and M. Parrinello, *Proc. Natl. Acad. Sci. U. S. A.*, 2013, **110**, 13723-13728.
75. P. L. Geissler, C. Dellago, D. Chandler, J. Hutter and M. Parrinello, *Science*, 2001, **291**, 2121-2124.
76. O. Rahaman, A. C. T. van Duin, W. A. Goddard and D. J. Doren, *J. Phys. Chem. B*, 2010, **115**, 249-261.
77. A. W. Lange and G. A. Voth, *J. Chem. Theory Comput.*, 2013, **9**, 4018-4025.
78. T. S. Hofer, M. Hitzenberger and B. R. Randolf, *J. Chem. Theory Comput.*, 2012, **8**, 3586-3595.
79. S. R. Billeter and W. F. van Gunsteren, *J. Phys. Chem. A*, 1998, **102**,

4669-4678.
80. T. S. Mahadevan and S. H. Garofalini, *J. Phys. Chem. B*, 2007, **111**, 8919-8927.
81. O. Schütt and D. Sebastiani, *J. Comput. Chem.*, 2013, **34**, 827-835.
82. L. Vilciauskas, S. J. Paddison and K.-D. Kreuer, *J. Phys. Chem. A*, 2009, **113**, 9193-9201.
83. G. Bekcioglu, C. Allolio, M. Ekimova, E. T. J. Nibbering and D. Sebastiani, *Phys. Chem. Chem. Phys.*, 2014, **16**, 13047-13051.
84. H. Azzouz and D. Borgis, *J. Chem. Phys.*, 1993, **98**, 7361-7374.
85. M. E. Tuckerman and D. Marx, *Phys. Rev. Lett.*, 2001, **86**, 4946-4949.
86. S. Hammes - Schiffer and J. C. Tully, *J. Chem. Phys.*, 1994, **101**, 4657-4667.
87. N. Uras-Aytemiz, J. P. Devlin, J. Sadlej and V. Buch, *Chem. Phys. Lett.*, 2006, **422**, 179-183.
88. J. A. Morrone, L. Lin and R. Car, *J. Chem. Phys.*, 2009, **130**, -.
89. S. Anderson, S. Crosson and K. Moffat, *Acta Crystallographica Section D*, 2004, **60**, 1008-1016.
90. D. A. Kraut, P. A. Sigala, T. D. Fenn and D. Herschlag, *Proc. Natl. Acad. Sci. U. S. A.*, 2010, **107**, 1960-1965.
91. R. A. Marcus, *J. Chem. Phys.*, 1965, **43**, 679-701.
92. A. Warshel and N. Barboy, *J. Am. Chem. Soc.*, 1982, **104**, 1469-1476.
93. T. C. Swinney and D. F. Kelley, *J. Chem. Phys.*, 1993, **99**, 211-221.
94. U. Drehmann, U. Pürschel and H. Wauschkun, *J. Prakt. Chem.*, 1961, **14**, 122-126.
95. P. E. Fanta, *Organic Syntheses*, 1952, **32**, 95-96.
96. C. Mundy, F. Mohamed, F. Schiffman, G. Tabacchi, H. Forbert, W. Kuo, J. Hutter, M. Krack, M. Iannuzzi and M. McGrath, http://www.cp2k.org/2000.
97. B. G. Lippert, J. H. Parrinello and Michele, *Mol. Phys.*, 1997, **92**, 477-488.
98. S. Grimme, *J. Comput. Chem.*, 2006, **27**, 1787-1799.
99. A. D. Becke, *Phys. Rev. A*, 1988, **38**, 3098-3100.
100. C. Lee, W. Yang and R. G. Parr, *Phys. Rev. B*, 1988, **37**, 785-789.
101. S. Goedecker, M. Teter and J. Hutter, *Phys. Rev. B*, 1996, **54**, 1703-1710.
102. G. Bussi, D. Donadio and M. Parrinello, *J. Chem. Phys.*, 2007, **126**, -.
103. M. J. Frisch, G. W. Trucks, H. B. Schlegel, G. E. Scuseria, M. A. Robb, J. R. Cheeseman, G. Scalmani, V. Barone, B. Mennucci, G. A. Petersson, H. Nakatsuji, M. Caricato, X. Li, H. P. Hratchian, A. F. Izmaylov, J. Bloino, G. Zheng, J. L. Sonnenberg, M. Hada, M. Ehara, K. Toyota, R. Fukuda, J. Hasegawa, M. Ishida, T. Nakajima, Y. Honda, O. Kitao, H. Nakai, T. Vreven, J. Montgomery, J. A., J. E. Peralta, F. Ogliaro, M. Bearpark, J. J. Heyd, E. Brothers, K. N. Kudin, V. N. Staroverov, R. Kobayashi, J. Normand, K. Raghavachari, A. Rendell, J. C. Burant, S. S. Iyengar, J. Tomasi, M. Cossi, N. Rega, J. M. Millam, M. Klene, J. E. Knox, J. B. Cross, V. Bakken, C. Adamo, J. Jaramillo, R. Gomperts, R. E. Stratmann, O. Yazyev, A. J. Austin, R. Cammi, C. Pomelli, J. W. Ochterski, R. L. Martin, K. Morokuma, V. G. Zakrzewski, G. A. Voth, P. Salvador, J. J. Dannenberg, S. Dapprich, A. D. Daniels, Ö. Farkas, J. B. Foresman, J. V. Ortiz, J. Cioslowski and D.

J. Fox, Gaussian Inc. Wallingford CT 2009.
104. W. Humphrey, A. Dalke and K. Schulten, *J. Mol. Graphics*, 1996, **14**, 33-38.
105. M. Brehm and B. Kirchner, *J. Chem. Inf. Model.*, 2011, **51**, 2007-2023.
106. K. L. Schuchardt, B. T. Didier, T. Elsethagen, L. Sun, V. Gurumoorthi, J. Chase, J. Li and T. L. Windus, *J. Chem. Inf. Model.*, 2007, **47**, 1045-1052.
107. D. Feller, *J. Comput. Chem.*, 1996, **17**, 1571-1586.
108. C. Adamo and V. Barone, *J. Chem. Phys.*, 1999, **110**, 6158-6170.
109. W. Kutzelnigg, U. Fleischer and M. Schindler, in *Deuterium and Shift Calculation*, Springer Berlin Heidelberg1991, vol. 23, ch. 3, pp. 165-262.
110. J. Guo, P. M. Tolstoy, B. Koeppe, G. S. Denisov and H.-H. Limbach, *J. Phys. Chem. A*, 2011, **115**, 9828-9836.
111. P. M. Tolstoy, J. Guo, B. Koeppe, N. S. Golubev, G. S. Denisov, S. N. Smirnov and H.-H. Limbach, *J. Phys. Chem. A*, 2010, **114**, 10775-10782.
112. B. Koeppe, doctor rerum naturalium PhD thesis, Freie Universität Berlin, 2011.

For Table of Contents Only

Graphical abstract

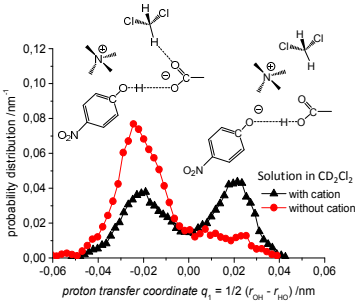

Textual abstract

The polar aprotic solvent fluctuations in the first solvation shell lead to a double-well potential and proton tautomerism in a low-barrier hydrogen bond.